Journal of Nuclear Materials 378 (2008) 188–192

Contents lists available at ScienceDirect

Journal of Nuclear Materials

journal homepage: www.elsevier.com/locate/jnucmat

Frenkel pair accumulation induced crystallization of amorphous $MgAl_2O_4$

Alain Chartier [a,*], Tomokazu Yamamoto [a,b], Kazuhiro Yasuda [b], Constantin Meis [c], Syo Matsumura [b]

[a] CEA-Saclay, DEN/DANS/DPC/SCP/LM2T, bât. 450 Sud, 91191 Gif-Sur-Yvette, France
[b] Department of Applied Quantum Physics and Nuclear Engineering, Kyushu University, 744 Motooka, Nishi-ku, Fukuoka 819-0395, Japan
[c] CEA-Saclay, INSTN/UESMS, bât. 395, 91191, Gif-Sur-Yvette, France

ARTICLE INFO

Article history:
Received 5 May 2008
Accepted 10 June 2008

PACS:
61.80.−x
61.43.Bn
81.30.−t

ABSTRACT

The epitaxial and homogeneous irradiation induced re-crystallization of amorphous $MgAl_2O_4$ was studied by means of continuous Frenkel pair accumulation in the molecular dynamics framework. Present results point out that the re-crystallization induced by Frenkel pair accumulation appears in both cases to be thermally enhanced but non diffusive. It is governed by a local rearrangement of each point defect in the homogeneous case, while spontaneous Frenkel pair recombination process in the crystalline part or at the interface drives the re-crystallization in the epitaxial case.

1. Introduction

Magnesium aluminate spinel $MgAl_2O_4$ is considered in the nuclear industry as a potential inert matrix for minor actinides incineration [1] due to its excellent radiation resistance. Radiation-induced behavior has been studied extensively using both experimental techniques [2–6] and recently numerous atomic scale modeling [7,8]. It has been observed that the amorphous (A) state may re-crystallize into a defective rock salt (NaCl) structure under electron irradiation [9]. The re-crystallization has been observed to occur both at the amorphous/crystalline interface by epitaxial (E) growth or directly in the A region by nucleation and growth.

Radiation induced crystallization from amorphous state may play a decisive role in the radiation resistance of materials. In fact, it has been observed [10] that the irradiation flux and temperature may be tuned to bring on either ion beam induced epitaxial crystallization (IBIEC) or ion beam induced interfacial amorphization (IBIIA). The rationalization of IBIEC has been done first by using the classical nucleation and growth theory [11] and then recently with microscopic models [12] based on the balance between the evolution of crystallization due to point defects produced by irradiation and the *diffusive* Frenkel pair (FP) recombination. The effect of ballistic displacements induced by radiation is often invoked as a driving process for the re-crystallization [9] at low temperature. This effect is nevertheless not included in current models.

In this study, we precisely focused on the ballistic displacements effect upon the homogeneous and epitaxial re-crystallization of amorphous spinel under *non-diffusive* annealing condition. The non diffusive annealing may be due to the spontaneous Frenkel pair recombination process or the local relaxation of point defects. The ballistic displacements were simulated by continuous cation Frenkel pair (FP) accumulation in the molecular dynamics (MD) framework.

2. Spinel structures

At low temperature the normal spinel (N-spinel) crystallizes in the Fd3m (227) space group. The magnesium ions are at the tetrahedral sites 8a while the aluminum ions are at the 16d octahedral sites. The oxygen ions are organized as an fcc sub-lattice in the 32e sites (see Figs. 1 and 2). Upon increase of temperature, the cation sublattices are disordered [14]; with anti-sites i.e. Mg/Al site inversion. The perfect disordering in the cation sub-lattice is attained for $x = 2/3$ in $Mg_{1-x}Al_x(Al_{2-x}Mg_x)O_4$. This will be referred as the disordered spinel (D-spinel). When all the Mg ions lie in the 16d octahedral sites, the tetrahedral sites being filled by Al cations, the structure is called as inverse spinel (I-spinel) and can be written as $Al[MgAl]_2O_4$ [15]. Note that the oxygen ions keep their own site 32e.

As already mentioned, a defective rocks-salt structure has been observed under electron irradiation. It can be described using the other fcc sub-lattice built up by the 16c sites (see Figs. 1 and 3). Both interpenetrating fcc sub-lattices 16c and 16d and the 32e sub-lattice form a defective rock salt structure when the Al and Mg cations are randomly distributed in the 16c and 16d sites.

Finally, there are two other tetrahedral special sites (48f and 8b, see Fig. 1), that are interstitial sites for spinel as well as for the defective rock salt structure. They mainly remain empty during all the simulations performed; and will not be considered in the following.

* Corresponding author. Tel.: +33 1 6908 3168; fax: +33 1 6908 9221.
E-mail address: alain.chartier@cea.fr (A. Chartier).

0022-3115/$ - see front matter © 2008 Elsevier B.V. All rights reserved.
doi:10.1016/j.jnucmat.2008.06.027

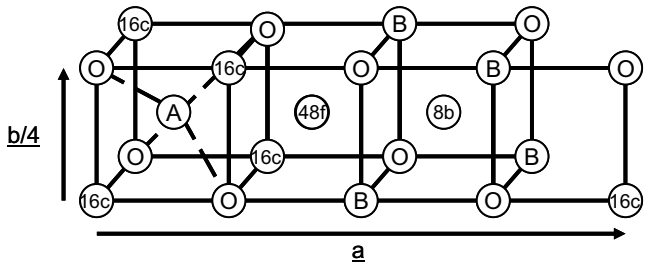

Fig. 1. Schematic representation of the partial spinel structure in the (100) plane. The (a) and (b) symbols indicate the axis of the conventional cell. The A, B and oxygen (O) sites of the N spinel are plotted (see the text for details) along with the octahedral vacancies (16c) and tetrahedral vacancies (8b and 48f).

3. Simulations details

3.1. Molecular dynamics simulation of the states of references

The study was done in the framework of empirical potentials molecular dynamic (MD) simulations with the two-body short-range ionic interactions fitted by Morooka et al. [16]. They are composed of a Buckingham potential and a Morse potential that complete the Coulomb interactions. Those potentials properly describe the thermal expansion as well as the elastic properties as a function of temperature for $MgAl_2O_4$, but also for the end-members MgO and Al_2O_3.

We further checked Morooka's potentials by evaluating the relative energies of the different solid state phases that may appear in $MgAl_2O_4$ under irradiation. This evaluation is necessary as unphysical stability between the different phases may lead to unphysical evolution of the structure under Frenkel pair accumulation. For example, the structure may spontaneously transit towards the amorphous state under FP accumulation if its relative energy is lower than the N-spinel. The physical properties as well as the radial distribution functions obtained for each phase of spinel will also be used as references for the on-line analysis of the evolution of the structure during the accumulation of FP.

We used super-cells built up by doubling the lattice parameter of the conventional cell along the three crystallographic directions, obtaining a 448-ion cell, except for the case of epitaxial re-crystallization. Thirty (30) different random configurations of the I-spinel, D-spinel and NaCl-spinel were generated and the lattices were relaxed by static energy minimization. Their relative energies, volumes and bulk modulus, were obtained by averaging over the thirty different configurations. We have also calculated the physical properties of the amorphous spinel (A-spinel). It was generated

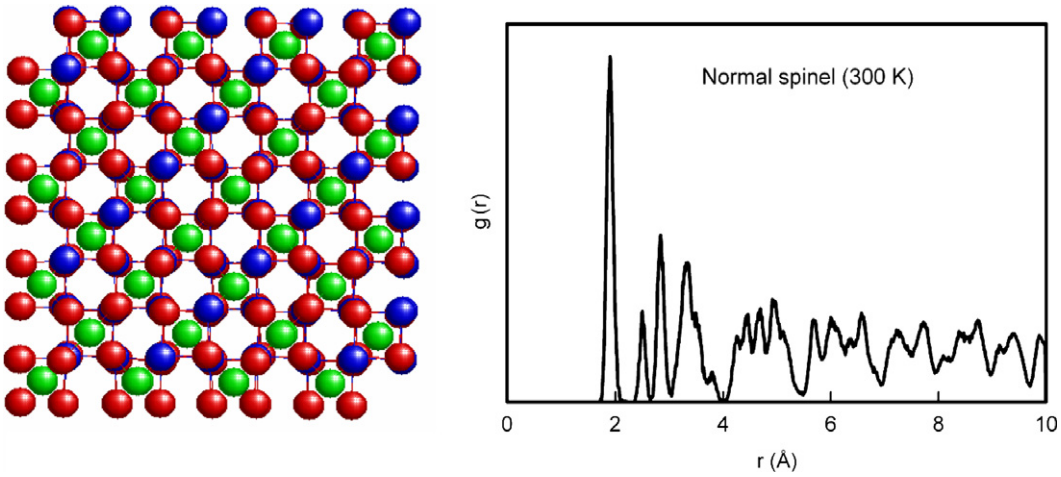

Fig. 2. Structure of the normal spinel from a [001] direction (left side) and the total radial distribution function calculated at 300 K (right side). Red, blue and green spheres represent oxygen, aluminum and magnesium, respectively. (For interpretation of the references to colour in this figure legend, the reader is referred to the web version of this article.)

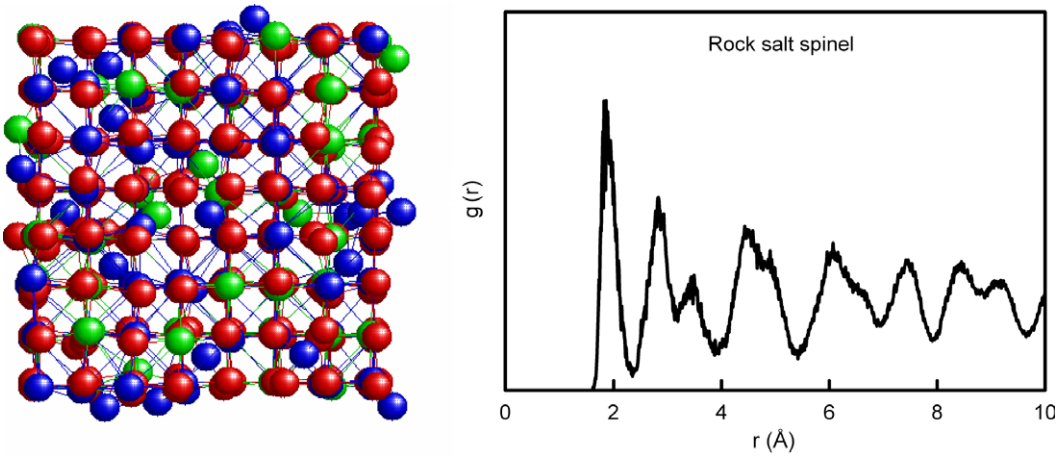

Fig. 3. Structure of the rock salt spinel from a [001] direction (left side) and the total radial distribution function calculated at 300 K (right side). See Fig. 2 for the definition of symbols.

by quenching a 448-atom super-cell from 6000 K towards 300 K with a linear cooling rate of 10 K/ps at constant pressure. This last method has been demonstrated to be suitable [17] for the A states generation. The properties of the A-spinel at 0 K were then calculated by static energy minimizations of the obtained A structure at 300 K.

The calculated relative energies of the different phases of spinel have been reported on Table 1. The N-spinel is the most stable, while the A structure is the least stable state. The calculated values are also in agreement with the available *ab initio* data [18]. Furthermore, we got consistent evolution of the bulk modulus, with a clear decrease for the A-spinel. As for the volume, it shrinks starting from N-spinel towards the I-spinel. More details on the relative stability of the four different crystalline states are available in a separate paper [19]. Concerning the A-spinel, the swelling is underestimated (+2.3%) when compared with various experimental values obtained at different irradiations conditions [20], being roughly 20%. Notice that Yu et al. [9] observed a shrinkage of about 10% when A-spinel is re-crystallized into a NaCl structure. The corresponding calculated value here is 3.6%. Finally, the bulk modulus of A-spinel is by far lower than that of the N-spinel, in agreement with the elastic softening due to amorphization observed by Devanathan [21].

The N-, NaCl- and A-spinel calculated structures and their total radial distribution functions (RDF) were reported on Figs. 2–4. Visual inspection from a [0 0 1] direction shown in the three figures is sufficient to identify the structures. The NaCl-spinel shows almost no cation in tetrahedral sites that makes a clear difference with the N-spinel. Of course, the A-spinel shows no apparent structure which can be easily identified visually. The total RDF of N-spinel, NaCl-spinel and A-spinel are very different from each other, too. The N-spinel shows sharper peaks compared to the NaCl-spinel. The total RDF of the A-spinel (Fig. 4) is almost flat for distances higher than 4 Å, as expected. Those differences will be used for the on-line analysis of these states.

In summary the relative energies, the total radial distribution function and the visual inspection of the structure may be used to identify the transition of the spinel structure under cation Frenkel pair accumulation.

Table 1
Physical properties of the different phases of spinel calculated using static energy minimization

	Volume (Å^3)	Bulk modulus (GPa)	Energy (eV/ion)	Energy (eV/ion) *Ab initio* [18]
Normal (N)	519.60	192.5	0.000	
Disordered (D)	516.60 (−0.3%)	193.7 (+0.6%)	0.047	*0.036*
Inverse (I)	514.30 (−1.0%)	202.0 (+4.9%)	0.054	*0.039*
Rock salt (NaCl)	512.97 (−1.3%)	153.4 (−20%)	0.144	
Amorphous (A)	531.60 (+2.3%)	139.9 (−27%)	0.183	

The properties were averaged over thirty (30) random configurations for D-spinel, I-spinel and NaCl-spinel. The normal (N)-spinel has been taken as a reference for the energy differences between states. The percentages refer to N-spinel structure.

3.2. Re-crystallization simulations

We have used two different starting states for the re-crystallization process induced by Frenkel pair (FP) accumulation. The starting structure for the homogeneous re-crystallization was a 448-ion A-spinel previously obtained by quenching using the procedure already described. The A-spinel was checked to be stable in the temperature range of 30–1800 K for simulation time of 1 ns. An 896-ion super-cell composed of half A-spinel and half NaCl-spinel volumes was used for simulating the epitaxial re-crystallization. We use the NaCl-spinel instead of the N-spinel ground state structure as it has been shown elsewhere [19] that the steady state under FP accumulation is the NaCl-structure. This interfacial configuration was confirmed to be stable in the temperature range of 30–1000 K for a simulation time of 1 ns.

The irradiation induced re-crystallization of the amorphous states of $MgAl_2O_4$ has been simulated by means of continuous cation FP creation in the amorphous phase and on the interfacial configuration with MD simulations in the NPT ensemble, using a method similar to the one used by Crocombette et al. [13]. In both cases, the cation Frenkel pairs are introduced one after another. For each FP introduction, one cation was randomly chosen and was displaced (its coordinates *only* were changed) randomly to an interstitial site. In the amorphous spinel, the interstitial is defined as a site located further than 1 Å distance from any other atoms of the cell. This process was done in the temperature ranges defined above, depending on the starting configurations. The target temperature was strictly maintained using a Nosé-Hoover thermostat in order to remove the excess of thermal energy produced by the introduction of FPs in the system. Such a method avoids any local heating caused by the FP production in the cell throughout the simulations. We assumed 1 ps and 10 ps for the time intervals between subsequent FP introductions. They correspond, respectively, to dose rates Φ of 5×10^9 and 5×10^8 displacements per cation per second (dpc/s) for a 448-atom cell. Those values of Φ are far higher

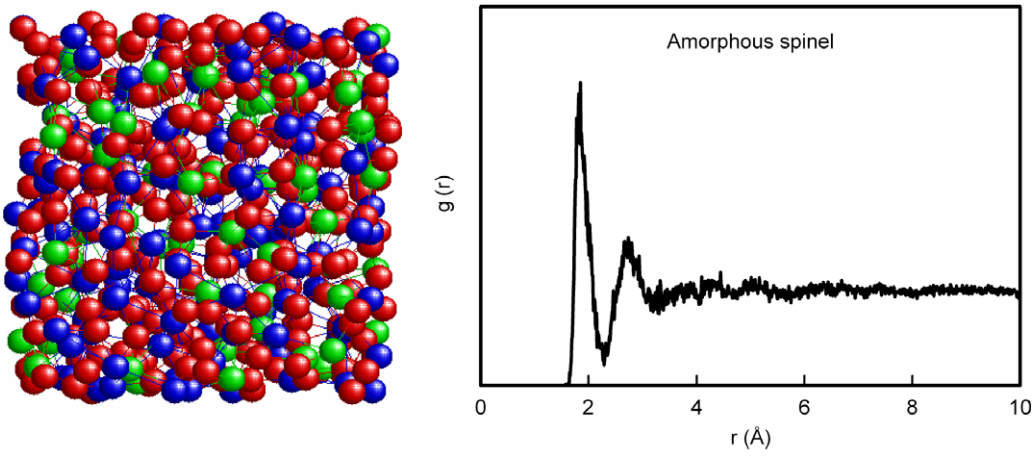

Fig. 4. Structure of the amorphous spinel from a [0 0 1] direction (left side) and the total radial distribution function calculated at 300 K (right side). See Fig. 2 for the definition of symbols.

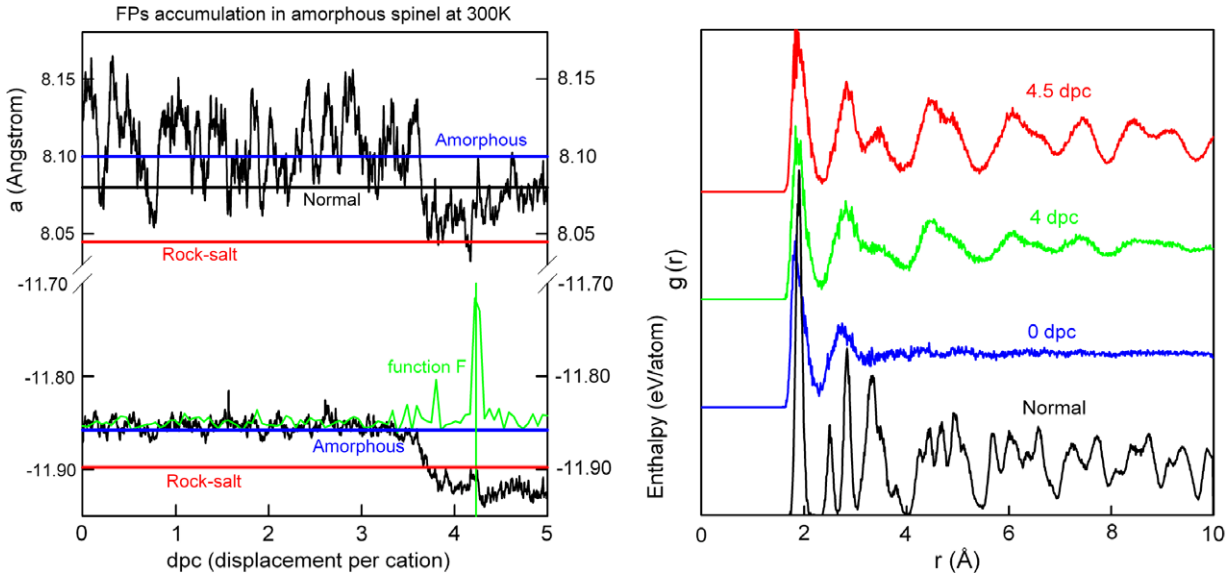

Fig. 5. Left: Evolution of the cell parameter (black line at the top of the figure), radial distribution correlation function F (green line, shifted and renormalized to meet the required scale, see the text for the definition) and enthalpy (black line at the bottom figure) as a function of the dose σ (in dpc, displacement per cation), for a dose rate ϕ of 5×10^9 dpc/s, starting at 0 dpc, from the A state of the spinel at 300 K. The black, green and red horizontal lines indicate the reference enthalpy (bottom) and cell parameter (top) values for N-, NaCl- and A-spinel, respectively. The homogeneous re-crystallization is indicated by the vertical green line at 4.2 dpc. Right part: radial distribution function (RDF) of N-spinel and A-spinel at different doses corresponding to the left part. At 0 dpc, spinel is in the A state, while it is in the NaCl structure at 4.5 dpc. (For interpretation of the references to colour in this figure legend, the reader is referred to the web version of this article.)

than the maximum dose rate that may be attained in experiments (10^{-3} dpa/s). Such short time intervals between FP introductions prohibit any long range migration, while it allows the FP to recombine spontaneously or to relax each defect locally. The analysis of the evolution of the cell structure as a function of dose D was done just before each FP creation. The structure analyzed is consequently the one obtained after relaxation of the previous FP creation during the interval of FP introduction. The transition of the structure was identified first by visual inspection, as the different phases may be easily identified (see Figs. 2–4). The analysis of the structure was checked by following the evolution of the enthalpy and the cell parameter (or the cubic root of the volume) as a function of dose. We also cross-controlled the analysis using the total radial distribution function (RDF). The average RDF was calculated by averaging 10 different analysis steps before the concerned value of dpc. The full crystallization of the cell was deduced by calculating the difference between the averaged RDF shifted by 10 times the period, using the following function F:

$$F(t) = \int_{r=0}^{10} \left| \sum_{i=1}^{10} \mathrm{RDF}(r, t+i+10)/10 - \sum_{i=1}^{10} \mathrm{RDF}(r, t+i)/10 \right| \mathrm{d}r,$$

where r is the radius (in Angström) of the RDF, t is the time (in period of FP introduction). Such a function $F(t)$ remains constant when the RDF is unchanged as a function of time. It shows a peak when a change occurs in the RDF (e.g. transition from A- towards NaCl-spinel, see Fig. 5 for an illustration).

4. Crystallization induced by Frenkel pair accumulation

At all the temperatures considered (i.e. from 30 to 1800 K) and whatever the FP production rate Φ considered, the A state of $MgAl_2O_4$ homogeneously re-crystallizes in the NaCl state when submitted to FP accumulation beyond a critical dose quoted D_C. As an example, one may observe in Fig. 5 (left part) the evolution and transition of the enthalpy, the cell parameter and the function F as a function of σ when FP are accumulated with 1 ps intervals at 300 K in the A state. The total energy as well as the cell parameter oscillates during the FP accumulation up to 3.6 dpc, since some very energetically unfavorable FP increase the both parameter for very short time. The corresponding RDF during the accumulation regime shows the A state (as an example is shown in Fig. 5 right part and quoted as 0 dpc for the starting A state). For both energy and cell parameter, there is a clear transition at around 3.6 dpc to some energetically more stable state. The small peak at 3.6 dpc of the function F indicates that this state takes a local crystallographic modification. The corresponding RDF (4 dpc in Fig. 5) indicates that the structure is partly crystallized since some peaks appear in the range $r < 8$ Å. Visual inspection of the structure shows that some parts of the super-cell contained small NaCl type crystallites with grain boundaries between them. The main crystallographic transition from the A state towards a full NaCl super-cell occurs at 4.2 dpc, as the function F draws a significant peak. The RDF function at 4.5 dpc (Fig. 5) shows more extended structural correlation over 10 Å. This crystalline state remains stable when subsequently submitted to FP accumulations up to 10 dpc. This result along with the results obtained in Ref. [19] confirms that a steady state crystalline NaCl type structure has been obtained under continuous accumulations of cation FP. This assertion is true in the present simulation whatever the temperature or the dose rate considered.

Since a NaCl type crystal is obtained by the homogeneous re-crystallization, we next considered the epitaxial re-crystallization of the A-spinel on the NaCl-spinel. Re-crystallization towards the NaCl state was also obtained beyond a certain dose of FP accumulation, at all the temperatures considered. No small crystallites where detected in any of those epitaxial cases.

Using the criteria mentioned above for the re-crystallization detection, the values of D_C for the two different FP production rates were obtained as a function of temperature, as shown in Fig. 6 for the H (homogeneous) case and the E (epitaxial) one. A clear trend appears that D_C decreases with temperature. We recall that the re-crystallization observed in the present simulations both for the H and the E cases is not induced by any local heating since the target temperature is strictly maintained and since the A states are stable at temperatures considered for both H and E cases. No thermal

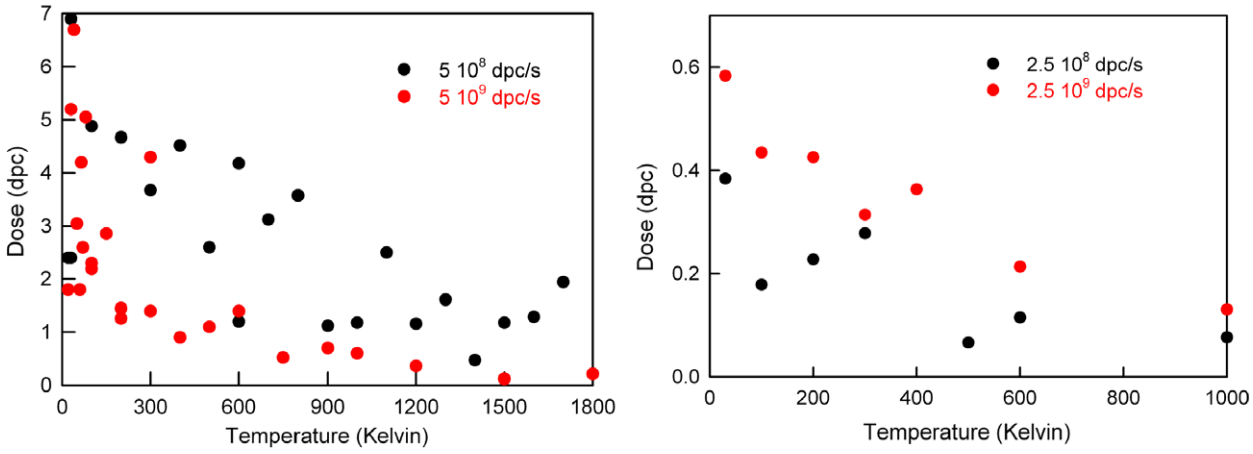

Fig. 6. Dose of re-crystallization of the A-spinel (homogeneous (H) case; left part) and of the epitaxial amorphous/ crystal spinel (epitaxial (E) case; right part) as a function of temperature.

diffusion of the point defects is allowed as the period of FP introduction is too short (whether 1 or 10 ps). It means that thermally activated crystallization rate and/or thermally activated annealing (whether Frenkel pair recombination or local reorganization) contribute to the re-crystallization process.

Furthermore, we can compare the homogeneous and epitaxial re-crystallization doses D_C, as the amorphous volume re-crystallized is the same (448-atom amorphous cell) in both cases. One can observe in Fig. 6 that the values of D_C are far lower in the E case than in the H case. This is consistent with the fact that experimental observation of H re-crystallization is very seldom. It also means that E and H re-crystallization may be interpreted independently in the present simulations. The other main characteristic of those results is that the critical doses D_C for re-crystallization depend upon the FP production rate Φ. The higher Φ requires the lower D_C in the H case ($D_C \propto \Phi^{\beta}$ with $0 < \beta < 1$). This trend is reversed in the E case ($D_C \propto 1/\Phi^{\beta}$ with $\beta > 1$). It is, therefore, straightforward that different microscopic mechanisms pilot the re-crystallization of spinel in the homogeneous nucleation and growth and in the epitaxial processes. Following the proposed model from Heera et al. [12] (equation 15 in their paper), we may deduce that homogeneous re-crystallization is driven by the local reorganization induced by the cation displacements while in the epitaxial case the re-crystallization is governed by the Frenkel pair annealing.

5. Conclusion

We have shown in the present work that the homogeneous and epitaxial irradiation induced re-crystallization can be simulated by means of Frenkel pair accumulations in the molecular dynamics simulation framework. The re-crystallization observed in the present simulations is not induced by any local heating since the target temperature is strictly maintained and since the A states are temperature stable for both homogeneous (H) and epitaxial (E) cases. Furthermore, no thermal diffusion of the point defects was allowed since the periods considered for Frenkel pair introduction are too short (1 or 10 ps). Consequently, ballistic displacements counteracted by *non diffusive* annealing are the mechanisms that kinetically induce the re-crystallization. This is consistent with the suggestion advanced by Yu et al. [9]. Finally, we have identified the different microscopic mechanisms that govern the homogeneous and the epitaxial re-crystallization. The first one is mainly driven by local independent point defects reorganization, comparable the observation done by Delaye and Limoge in a Lennard-Jones glass [22] while the last one is rather driven by FP recombination.

Acknowledgements

T.Y. and A.C. would like to thank the support to their exchange and stays by CEA-Saclay and Kyushu University. This work was partly supported by Grant-in-Aid for Scientific Research (A) (Grant No. 18206068) from Japan Society for the Promotion of Science (JSPS) and by a grant from Egide Foundation, Paris, France. Parts of the calculations were done in CEA-Saclay using the Godunov cluster (DSM/INSTN).

References

[1] Hj. Matzke, V.V. Rondinella, T. Wiss, J. Nucl. Mater. 274 (1999) 47.
[2] K.E. Sickafus, C.J. Wetteland, N.P. Baker, N. Yu, R. Devanathan, M. Nastasi, N. Bordes, Mater. Sci. Eng. A 253 (1998) 78.
[3] T. Soeda, S. Matsumura, C. Kinoshita, N.J. Zaluzec, J. Nucl. Mater. 283&287 (2000) 952.
[4] D. Simeone, C. Dodane-Thiriet, D. Gosset, P. Daniel, M. Beauvy, J. Nucl. Mater. 300 (2002) 151.
[5] M. Shimada, S. Matsumura, K. Yasuda, C. Kinoshita, Y. Chimi, N. Ishikawa, A. Iwase, J. Nucl. Mater. 329&333 (2004) 1446.
[6] T. Wiss, H. Matzke, V.V. Rondinella, T. Sonoda, W. Assmann, M. Toulemonde, C. Trautmann, Prog. Nucl. Energ. 38 (2001) 281.
[7] D. Bacorisen, R. Smith, J.A. Ball, R.W. Grimes, B.P. Uberuaga, K.E. Sickafus, W.T. Rankin, Nucl. Instr. and Meth. B 250 (2006) 36.
[8] S.P. Chen, M. Yan, J.D. Gale, R.W. Grimes, R. Devanathan, K.E. Sickafus, N. Yu, M. Nastasi, Phil. Mag. Lett. 73 (1996) 51.
[9] N. Yu, K.E. Sickafus, M. Nastasi, Mater. Chem. Phys. 46 (1996) 161.
[10] E. Wendler, N. Dharmarasu, E. Glaser, Nucl. Instr. and Meth. B 160 (2000) 257.
[11] P. Bruna, D. Crespo, R. González-Cinca, J. Appl. Phys. 100 (2006) 54907.
[12] V. Heera, T. Henkel, R. Kögler, W. Skorupa, Phys. Rev. B 52 (1995) 15776.
[13] J.-P. Crocombette, A. Chartier, W.J. Weber, Appl. Phys. Lett. 88 (2006) 51912.
[14] W.E. Gorter, Philips Res. Rep. 9 (1954) 403.
[15] K.E. Sickafus, J.M. Wills, N.W. Grimes, J. Am. Ceram. Soc. 82 (1999) 3279.
[16] S. Morooka, S. Zhang, T. Nishikawa, H. Awaji, J. Ceram. Soc. Jpn. 107 (1999) 1225.
[17] L.R. Corrales, J. Du, Phys. Chem. Glasses 46 (2005) 420.
[18] A. Seko, K. Yuge, F. Oba, A. Kuwabara, I. Tanaka, Phys. Rev. B B73 (2006) 94116.
[19] T. Yamamoto, A. Chartier, K. Yasuda, C. Meis, K. Shiiyama, S. Matsumura, Nucl. Instr. and Meth. B 266 (2008) 2676.
[20] T. Wiss, Hj. Matzke, Radiat. Measur. 31 (1999) 507.
[21] R. Devanathan, N. Yu, K.E. Sickafus, M. Nastasi, J. Nucl. Mater. 232 (1996) 59.
[22] J.M. Delaye, Y. Limoge, J. Phys. I 3 (1993) 2063;
J.M. Delaye, Y. Limoge, J. Phys. I 3 (1993) 2079.